Relativistic spin-density-functional theory: Robust solution of single-particle equations for open-subshell atoms

E. Engel, T. Auth, and R. M. Dreizler
Institut für Theoretische Physik, J. W. Goethe Universität Frankfurt, D-60054 Frankfurt/Main, Germany
(Received 23 May 2001; published 29 November 2001)

We present an approach to the solution of the collinear form of the single-particle equations of relativistic spin-density-functional theory. It is based on the use of appropriate boundary conditions for $r\to 0,\infty$ and the identification of ''spin-up'' and ''spin-down'' solutions by a node quantum number. A comparison with previous results and a complete set of reference data for atomic ground states is provided.

DOI: 10.1103/PhysRevB.64.235126 PACS number(s): 71.15.Mb, 71.15.Rf, 31.10.+z

I. INTRODUCTION

A relativistic spin-density-functional theory (RSDFT) for magnetic systems was introduced by MacDonald and Vosko[1] and Ramana and Rajagopal[2] more than 20 years ago. The basic variables of this formalism are the charge density $n(\boldsymbol{r})$ and the magnetization density $\boldsymbol{m}(\boldsymbol{r})$ (we will nevertheless often use the term ''spin,'' rather than ''magnetization,'' in spite of the fact that the notion of spin is no longer well defined). RSDFT can be derived from the more general, QED-based four current version of relativistic density-functional theory[3,4] by neglecting the coupling between the orbital part of the spatial current $\boldsymbol{j}$ and the external vector potential $\boldsymbol{V}_{ext}$;

$$-\frac{e}{c}\int d^3r\, \boldsymbol{j}\cdot\boldsymbol{V}_{ext}\to\int d^3r\, \boldsymbol{m}\cdot\boldsymbol{B}_{ext}.$$

On the other hand, for systems not subject to external magnetic fields, one can give RSDFT a rigorous foundation by considering the actual physical Hamiltonian with $\boldsymbol{B}_{ext}=\boldsymbol{0}$ as one element of a mathematically well-defined general set of Hamiltonians with the coupling $\int d^3r\, \boldsymbol{m}\cdot\boldsymbol{B}_{ext}$. The basic density-functional variables resulting from this type of Hamiltonian are $n(\boldsymbol{r})$ and $\boldsymbol{m}(\boldsymbol{r})$. As the Hamiltonian of interest is obtained in the limit $\boldsymbol{B}_{ext}\to\boldsymbol{0}$ from the more general Hamiltonian, $n(\boldsymbol{r})$ and $\boldsymbol{m}(\boldsymbol{r})$ are also legitimate variables in the case of the actual physical system, irrespective of the fact that for nonzero $\boldsymbol{B}_{ext}$ the underlying Hamiltonian differs from the correct QED Hamiltonian (For a more detailed discussion and a comparison of the various versions of relativistic density functional theory, see Ref. 5).

In general, the direction of $\boldsymbol{m}$ can vary with position. Corresponding ground states for which the direction of $\boldsymbol{m}$ either changes from site to site (interatomic noncollinear magnetism—see, e.g., Ref. 6) or even on the atomic scale (intraatomic noncollinear magnetism[7]) were found for a number of solids. However, the structure of the single-particle equations with fully noncollinear $\boldsymbol{m}$ is rather involved, so that only a limited number of corresponding applications is available to date.[7,8] In addition, noncollinearity turned out to be not very important for open-subshell atoms,[8] i.e., the single-site problem. For this reason the collinear form of RSDFT, in which the orientation of $\boldsymbol{m}$ is globally fixed as $\boldsymbol{m}=(0,0,m_z)$, represents the standard approach in DFT-based calculations for magnetic materials (see, e.g., Ref. 9).

With the assumption of collinearity, the single-particle equations of RSDFT read[2]

$$[-ic\boldsymbol{\alpha}\cdot\boldsymbol{\nabla}+(\beta-1)m_ec^2+v_s+\beta\Sigma_z B_{xc}]\phi_k=\epsilon_k\phi_k, \quad (1)$$

where the effective potentials are given by

$$v_s(\boldsymbol{r})=v_{ext}(\boldsymbol{r})+v_H(\boldsymbol{r})+v_{xc}(\boldsymbol{r}), \quad (2)$$

$$v_H(\boldsymbol{r})=e^2\int d^3r'\frac{n(\boldsymbol{r}')}{|\boldsymbol{r}-\boldsymbol{r}'|}, \quad (3)$$

$$v_{xc}(\boldsymbol{r})=\frac{\delta E_{xc}[n,m_z]}{\delta n(\boldsymbol{r})} \quad (4)$$

$$B_{xc}(\boldsymbol{r})=-\mu_B\frac{\delta E_{xc}[n,m_z]}{\delta m_z(\boldsymbol{r})}. \quad (5)$$

The charge and magnetization densities are evaluated as

$$n(\boldsymbol{r})=\sum_k \Theta_k\phi_k^\dagger(\boldsymbol{r})\phi_k(\boldsymbol{r}), \quad (6)$$

$$m_z(\boldsymbol{r})=-\mu_B\sum_k \Theta_k\phi_k^\dagger(\boldsymbol{r})\beta\Sigma_z\phi_k(\boldsymbol{r}), \quad (7)$$

$$\Theta_k=\begin{cases}0 & \text{for} \quad \epsilon_k\leqslant -m_ec^2\\ 1 & \text{for} \quad -m_ec^2<\epsilon_k\leqslant\epsilon_F\\ 0 & \text{for} \quad \epsilon_F<\epsilon_k,\end{cases} \quad (8)$$

where, as usual, the no-pair approximation has been applied. $E_{xc}[n,m_z]$ is the exchange-correlation (xc) energy functional of RSDFT, which, in principle, contains all effects of the transverse (retarded Breit) interaction, including the transverse Hartree energy.[10] In practice, however, the latter is consistently neglected, and we follow this standard.

The magnetization dependence of the relativistic $E_{xc}[n,m_z]$ was only investigated for the exchange contribution to the relativistic extension (RLDA) of the local-density approximation (LDA), $E_x^{RLDA}[n,m_z]$ (Refs. 2 and 11–13) (throughout this contribution the abbreviation LDA is also used for the spin-dependent functional, which is often termed

the LSDA in the literature). Moreover, while $E_x^{RLDA}[n,m_z]$ is known analytically in the case of unpolarized systems,[14,1] it is only available in tabulated form for polarized systems. Only the weakly relativistic limit of $E_x^{RLDA}[n,m_z]$ (to first order in $1/c^2$) was evaluated analytically by Xu *et al.*[13] (this functional is abbreviated by XRR in the following). Nothing is known about the m_z dependence of $E_c^{RLDA}[n,m_z]$. For this reason Eqs. (1)–(8) are usually applied in conjunction with nonrelativistic spin-density functionals $E_{xc}[n_\uparrow,n_\downarrow]$, which are adapted with the aid of

$$n_\pm(\boldsymbol{r})=\frac{1}{2}\left[n(\boldsymbol{r})\mp\frac{1}{\mu_B}m_z(\boldsymbol{r})\right] \tag{9}$$

$$v_{xc}(\boldsymbol{r})=\frac{1}{2}\left\{\frac{\delta E_{xc}[n_+,n_-]}{\delta n_+(\boldsymbol{r})}+\frac{\delta E_{xc}[n_+,n_-]}{\delta n_-(\boldsymbol{r})}\right\}, \tag{10}$$

$$B_{xc}(\boldsymbol{r})=\frac{1}{2}\left\{\frac{\delta E_{xc}[n_+,n_-]}{\delta n_+(\boldsymbol{r})}-\frac{\delta E_{xc}[n_+,n_-]}{\delta n_-(\boldsymbol{r})}\right\}. \tag{11}$$

Besides nonrelativistic LDA functionals, the more advanced generalized gradient approximation (GGA)[15] can be employed. Equations (9)–(11) also provide the basis for a semirelativistic approach, in which the relativistic LDA or GGA (Ref. 16) exchange for unpolarized systems is combined with the spin dependence of the nonrelativistic exchange functional (as the application of completely nonrelativistic xc functionals, this scheme implies errors of the order of $1/c^2$).

The solution of Eqs. (1)–(8) turns out to be far from simple even for open-subshell atoms. A first algorithm was presented by Cortona *et al.*,[17] and applied to triply charged positive ions of the lanthanide series. An alternative scheme, originally designed for the treatment of core states in band structure calculations, was suggested by Ebert.[18] Recently, two further algorithms were presented by Yamagami *et al.*[19] and Forstreuter *et al.*[20] As in the procedures by Cortona *et al.* and Ebert, the scheme of Yamagami *et al.* is based on finite-difference methods. The approach of Forstreuter *et al.*, on the other hand, relies on a basis set expansion.

The variety of algorithms suggested and the limited number of atomic results available in the literature reflects the intricate structure of Eq. (1), the main problem being a clear technical (and conceptual) distinction of ''spin-up'' and ''spin-down'' solutions. In this paper we suggest a robust algorithm for the solution of Eq. (1), which is based on the identification of an unambigous node quantum number for the distinction of spin-up and -down states. The scheme relies on finite-difference methods, so that any desired accuracy can be achieved by a suitable choice of the radial grid. It can be directly implemented in standard band structure codes (for the calculation of core states). Due to its high stability and the very general nature of the boundary conditions used, the algorithm allows calculations for any neutral atom, both on the level of the LDA as well as the numerically more critical GGA, employing either a point nucleus or an extended nuclear charge distribution. Taking the limit $c\rightarrow\infty$ in a numerical fashion, the usual nonrelativistic spin-density-functional results are reproduced with high accuracy.

The scheme is discussed in detail in Sec. II, with emphasis on the role of appropriate boundary conditions. A number of illustrative results and a comparison with the data in the literature are given in Sec. III, with a focus on transition-metal elements, lanthanides and actinides as cases of particular interest. In addition, we provide a complete set of atomic ground-state energies obtained with three frequently used xc functionals which can serve as atomic reference data for the evaluation of cohesive and dissociation energies in future applications of RSDFT. We summarize our results in Sec. IV.

II. SOLUTION OF SINGLE-PARTICLE EQUATIONS FOR OPEN-SUBSHELL ATOMS

The starting point for the discussion of open-subshell atoms in the framework of RSDFT is a suitable ansatz for the RSDFT spinors. The exact solution of Eq. (1) can be expanded in the forms

$$\phi_k(\boldsymbol{r})=\frac{1}{r}\sum_{ljm}\begin{pmatrix} a_k^{ljm}(r) & \Omega_{j,l,m}(\Theta,\varphi)\\ ib_k^{ljm}(r) & \Omega_{j,2j-l,m}(\Theta,\varphi)\end{pmatrix}, \tag{12}$$

$$\Omega_{jlm}=\sum_{m_l=-l}^{l}\sum_{s=\pm 1/2}\left\langle lm_l\frac{1}{2}s\middle|jm\right\rangle Y_{lm_l}(\Theta,\varphi)\chi_s, \tag{13}$$

i.e., in terms of basis functions which have the form of the standard eigenfunctions of closed-subshell atoms. Assuming spherical potentials, which implies a spherical averaging of the Hartree and xc components in v_s and of B_{xc}, one immediately finds that m is a good quantum number. One can also show that the coupling of states with different l is weak,[17] so that l can also serve as a ''good'' quantum number, and only states with different j (but the same m) remain coupled in expansion (12). In the final ansatz for ϕ_k one thus has to differentiate between states with $2|m|=2l+1$ (which includes s states), which have the standard form of closed-subshell spinors with $j=l+\frac{1}{2}$,

$$\phi_{nlm}(\boldsymbol{r})=\frac{1}{r}\begin{pmatrix} a_{nlm}(r) & \Omega_{l+(1/2),l,m}\\ ib_{nlm}(r) & \Omega_{l+(1/2),l+1,m}\end{pmatrix}, \tag{14}$$

and states with $2|m|\neq 2l+1$, for which a superposition of $j=l+\frac{1}{2}$ with $j=l-\frac{1}{2}$ spinors is used:[17]

$$\phi_{nlm\sigma}(\boldsymbol{r})=\frac{1}{r}\sum_{s=\pm 1}\begin{pmatrix} a_{nlm\sigma}^{s}(r) & \Omega_{l+(s/2),l,m}\\ ib_{nlm\sigma}^{s}(r) & \Omega_{l+(s/2),l+s,m}\end{pmatrix}. \tag{15}$$

In Eqs. (14) and (15), n represents the standard node quantum number. In addition, we have introduced a quantum number σ whose precise nature remains to be clarified. For closed-subshell atoms σ is equivalent to j, i.e., σ can take two values only.

Insertion of Eqs. (14) and (15) into Eq. (1) leads to two sets of coupled radial equations for the individual components. For states with $2|m|=2l+1$, this set is similar to the case of closed subshells ($k\equiv nlm$):

$$c\left(\partial_r - \frac{l+1}{r}\right)a_k = \left[2m_e c^2 - \left(v_s - \epsilon_k + \frac{2m}{2l+3}B_{xc}\right)\right]b_k, \tag{16}$$

$$c\left(\partial_r + \frac{l+1}{r}\right)b_k = \left(v_s - \epsilon_k + \frac{2m}{2l+1}B_{xc}\right)a_k. \tag{17}$$

For states with $2|m| \neq 2l+1$ one obtains[17] ($k \equiv nlm\sigma$)

$$c\left(\partial_r - \frac{l+1}{r}\right)a_k^+ = \left[2m_e c^2 - \left(v_s - \epsilon_k + \frac{2m}{2l+3}B_{xc}\right)\right]b_k^+, \tag{18}$$

$$c\left(\partial_r + \frac{l+1}{r}\right)b_k^+ = \left(v_s - \epsilon_k + \frac{2m}{2l+1}B_{xc}\right)a_k^+ + C_{lm}B_{xc}a_k^-, \tag{19}$$

$$c\left(\partial_r + \frac{l}{r}\right)a_k^- = \left[2m_e c^2 - \left(v_s - \epsilon_k - \frac{2m}{2l-1}B_{xc}\right)\right]b_k^-, \tag{20}$$

$$c\left(\partial_r - \frac{l}{r}\right)b_k^- = \left(v_s - \epsilon_k - \frac{2m}{2l+1}B_{xc}\right)a_k^- + C_{lm}B_{xc}a_k^+, \tag{21}$$

$$C_{lm} = -\frac{[(2l+1)^2 - (2m)^2]^{1/2}}{2l+1}. \tag{22}$$

Equations (16) and (17) can be solved with the standard techniques used for closed-subshell atoms, so that we focus on the solution of Eqs. (18)–(21) in the following.

For this solution we proceed in the standard fashion:[21] Starting from suitable boundary conditions at the origin the differential equations (18)–(21) are integrated outward for a trial value for ϵ_k (via some finite-difference scheme). For the same ϵ_k an inward integration is performed, starting from a sufficiently large radius r_{max}. The mismatch of the outward and inward integrated solutions at some intermediate radius R (typically the classical turning point) determines a correction for the eigenvalue. The three steps are then repeated until convergence is obtained.

The first step of the solution of Eqs. (18)–(21) is thus an analysis of the small-r regime, which fixes the boundary conditions for the outward integration. For this purpose one has to specify the behavior of the potentials in the vicinity of the nucleus:

$$v_s(r) = \frac{v_{-1}}{r} + v_0 + v_1 r + v_2 r^2 + \cdots, \tag{23}$$

$$B_{xc}(r) = B_0 + B_1 r + B_2 r^2 + \cdots. \tag{24}$$

The power series [Eqs. (23) and (24)] are exact for finite nuclei (with $v_{-1}=0$), and an excellent approximation for point nuclei: While the LDA and GGA xc potentials diverge at the origin in the case of point nuclei, this divergence is weak compared to the divergence of the nuclear potential, so that it can be absorbed into v_0 and B_0 (for GGA's the leading contribution may alternatively be included in v_{-1}). Note that B_0 does not vanish in general, as is easily seen for alkali- or noble-metal atoms (compare Sec. III). The small-r behavior of the four components of ϕ_k can then be extracted by insertion of Eqs. (23) and (24) into Eqs. (18)–(21). One finds two independent sets of coupled solutions for the components with one free coefficient in each of the sets. The first set is given by

$$a^+(r) = r^g a_0^+ + \cdots, \tag{25}$$

$$b^+(r) = \left[\frac{v_{-1}}{c}\frac{1}{g+l+1}\right]r^g a_0^+ + \cdots, \tag{26}$$

$$a^-(r) = \left[-\frac{C_{lm}}{2}\frac{B_0}{c}\frac{v_{-1}}{c}\frac{1}{g+l+1}\right]r^{g+1}a_0^+ + \cdots, \tag{27}$$

$$b^-(r) = \left[\frac{C_{lm}}{2}\frac{B_0}{c}\right]r^{g+1}a_0^+ + \cdots, \tag{28}$$

$$g = \sqrt{(l+1)^2 - \left(\frac{v_{-1}}{c}\right)^2}, \tag{29}$$

where a_0^+ has been chosen as free coefficient in order to ensure the stability of the algorithm in the limits $(v_{-1}/c) \to 0$ and $(B_0/c) \to 0$ (For brevity the quantum number k has been dropped). In the limit $B_{xc}=0$ this solution goes over into a $j=l+1/2$ state.

The second possible solution, for which b_0^- is the most appropriate choice for the free coefficient, has the forms

$$a^+(r) = \left[-\frac{C_{lm}}{2}\frac{B_0}{c}\right]r^{f+1}b_0^- + \cdots, \tag{30}$$

$$b^+(r) = \left[-\frac{C_{lm}}{2}\frac{B_0}{c}\frac{v_{-1}}{c}\frac{1}{f+l}\right]r^{f+1}b_0^- + \cdots, \tag{31}$$

$$a^-(r) = \left[-\frac{v_{-1}}{c}\frac{1}{f+l}\right]r^f b_0^- + \cdots, \tag{32}$$

$$b^-(r) = r^f b_0^- + \cdots, \tag{33}$$

$$f = \sqrt{l^2 - \left(\frac{v_{-1}}{c}\right)^2}. \tag{34}$$

This solution corresponds to a $j=l-1/2$ state for $B_{xc}=0$. Equations (25)–(29) and (30)–(34) can be used directly as coupled boundary conditions for the outward integration.[22] These boundary conditions differ from those suggested in Refs. 17–19 by a coupling of the + and − components via B_0.

In the next step one has to analyze Eqs. (18)–(21) for large r. In this limit the potentials behave as

$$v_s(r) = \frac{\overline{v}_{-1}}{r} + \frac{\overline{v}_{-2}}{r^2} + \cdots + \overline{v}_0 e^{-\gamma_1 r}, \tag{35}$$

$$B_{xc}(r) = \frac{\overline{B}_{-2}}{r^2} + \cdots + \overline{B}_0 e^{-\gamma_2 r}. \tag{36}$$

$\overline{v}_{-1}$ reflects a possible ionic charge and, in the case of the exact exchange functional, the self-interaction correction for the most weakly bound orbital.[10] In LDA or GGA calculations for neutral atoms, one has $\overline{v}_{-1}=0$. The quantities $\overline{v}_{-2}$ and $\overline{B}_{-2}$ vanish in the case of the LDA and for most GGA's, so that v_s and B_{xc} decay exponentially for neutral atoms. On the other hand, $1/r^2$ contributions are present for the Becke GGA.[23,24] Insertion of Eqs. (35) and (36) into Eqs. (18)–(21) shows that asymptotically a^+ and b^+ are decoupled from a^- and b^-:

$$a^{\pm}(r)=\overline{a}_0^{\pm} r^h e^{-\alpha r}, \tag{37}$$

$$b^{\pm}(r)=\left[\frac{\epsilon}{c\alpha}\right]\overline{a}_0^{\pm} r^h e^{-\alpha r}, \tag{38}$$

$$\alpha=[-\epsilon(2m_e+\epsilon/c^2)]^{1/2}, \tag{39}$$

$$h=-\frac{\overline{v}_{-1}}{c}\frac{m_e c^2+\epsilon}{[-\epsilon(2m_e c^2+\epsilon)]^{1/2}}. \tag{40}$$

One thus also finds two independent sets of boundary conditions with one free constant in each of the sets. For the first solution one chooses $\overline{a}_0^+$ as a free coefficient, and sets $\overline{a}_0^-$ equal to zero. For the second solution the role of the two coefficients is interchanged.

The decay of B_{xc} for large values of r is determined by the eigenvalues of the most weakly bound orbitals. Thus, in the case of core states, B_{xc} is not yet sufficiently small for typical starting points r_{max} for the inward integration. In addition, one has either $|a^+(r_{max})|\ll|a^-(r_{max})|$ or $|a^+(r_{max})|\gg|a^-(r_{max})|$, as the core states are close to spinors with good j. Consequently, at r_{max} the B_{xc} term which couples the dominant component a^{-s} to the much smaller component a^{+s} can be larger than the asymptotically leading contribution on the right-hand sides of Eqs. (19) and (21), $|C_{lm}B_{xc}a^{-s}|>|\epsilon a^{+s}|$. The asymptotic independence of a^+, b^+ from a^-, b^- is thus lost in many practical situations. Fortunately, an inclusion of the asymptotically leading B_{xc} contribution in the boundary conditions is possible (see the Appendix). For the first asymptotic solution this leads to

$$a^+(r)=\overline{a}_0^+ r^h e^{-\alpha r}, \tag{41}$$

$$b^+(r)=\left[\frac{\epsilon}{c\alpha}\right]\overline{a}_0^+ r^h e^{-\alpha r}, \tag{42}$$

$$a^-(r)=\left[\frac{\alpha C_{lm}}{2\epsilon}I(r)\right]\overline{a}_0^+ r^h e^{-\alpha r}, \tag{43}$$

$$b^-(r)=\left[\frac{C_{lm}}{2c}\left(I(r)-\frac{B_{xc}(r)}{\alpha}\right)\right]\overline{a}_0^+ r^h e^{-\alpha r}, \tag{44}$$

$$I(r)=\int_\infty^r dr' B_{xc}(r'). \tag{45}$$

For the second solution $+$ and $-$ have to be interchanged. Equations (41)–(44) can be used as boundary conditions for the inward integration for all Kohn-Sham (KS) states.

The complete solution of Eqs. (18)–(21) is then obtained by a linear combination of the two independent solutions from the outward and inward integrations:

$$a^s(r)=a^s_{1,out}(r)+a^s_{2,out}(r)=a^s_{1,in}(r)+a^s_{2,in}(r), \tag{46}$$

$$b^s(r)=b^s_{1,out}(r)+b^s_{2,out}(r)=b^s_{1,in}(r)+b^s_{2,in}(r). \tag{47}$$

The outward and inward integrated solutions have to be matched pairwise at some radius R. Use of three equations from the set of equations (46) and (47) at the matching point, together with the overall normalization of the spinor,

$$1=\int_0^\infty dr \sum_{s=\pm}[a^s(r)^2+b^s(r)^2], \tag{48}$$

allows a determination of the four free coefficients ($a^+_{1,out,0}$, $b^-_{2,out,0}$, $\overline{a}^+_{1,in,0}$, $\overline{a}^-_{2,in,0}$) in the boundary conditions. The remaining mismatch of the fourth equation then provides a first-order correction for the eigenvalue,

$$\begin{aligned}\delta\epsilon=c\sum_{s=\pm}&\{b^s_{out}(R)[a^s_{out}(R)-a^s_{in}(R)]-a^s_{out}(R)[b^s_{out}(R)\\&-b^s_{in}(R)]\}\Bigg[\int_0^R dr\sum_{s=\pm}[a^s_{out}(r)^2+b^s_{out}(r)^2]\\&+\int_R^\infty dr\sum_{s=\pm}[a^s_{in}(r)^2+b^s_{in}(r)^2]\Bigg]^{-1},\end{aligned} \tag{49}$$

where $a^+_{out}=a^+_{1,out}+a^+_{2,out}$ etc.

An important consequence of Eqs. (46) and (47) is the fact that the individual outward integrated solutions are not eigenstates of the RSDFT Hamiltonian. They thus must diverge exponentially for large r, as Eqs. (18)–(21) only allow exponentially decaying and exponentially increasing solutions. In view of Eqs. (46) and (47), the asymptotic divergencies must cancel between $a^s_{1,out}$ and $a^s_{2,out}$ as well as between $b^s_{1,out}$ and $b^s_{2,out}$. This is demonstrated in Fig. 1 for the first of the two $3d_{m=+3/2}$-type solutions of copper, for which a^- is the dominant component. A corresponding plot for the dominant component (a^+) of the second $3d_{m=+3/2}$-type solution of copper is given in Fig. 2. In both cases $a^s_{1,out}$ and $a^s_{2,out}$ start to diverge beyond the classical turning point, while their sum decays exponentially. There is, however, one important difference between the two solutions: The components of the energetically higher solution exhibit an additional node in the classically forbidden regime. This node allows an unambigous classification and a numerical distinction of the two states, which suggests an identification of the quantum number σ in Eq. (15) with the presence or absence of this feature. We will call the more weakly bound level the $\sigma=\downarrow$ state, and the level without any nodes in the classically forbidden regime the $\sigma=\uparrow$ state. In the example chosen the eigenvalues obtained with the nonrelativistic LDA for $E_{xc}[n_+,n_-]$ (Ref. 25) are -198.4 mH for the $3d^\uparrow_{m=+3/2}$

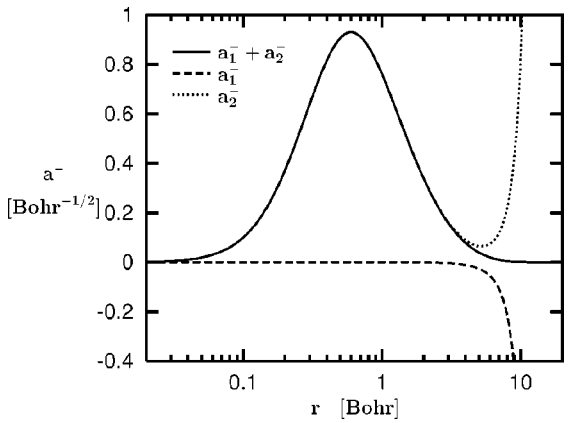

FIG. 1. Dominant component (a^-) of the $3d^{\uparrow}_{+3/2}$ state of Cu: Individual outward integrated solutions from boundary conditions (25)–(29) (a_1^-) and (30)–(34) (a_2^-) vs complete a^-.

state and -190.5 mH for the $3d^{\downarrow}_{m=+3/2}$ state. In the shooting procedure for the solution of Eqs. (18)–(21) the node in the classically forbidden regime can be used to obtain an upper or lower bound for the eigenvalue, analogous to the nodes in the classically allowed regime.

For a first illustration of the node quantum number σ we have chosen orbitals of a closed subshell. In this case one term in expansion (15) is highly dominant and very close to the corresponding spinor of the unpolarized approach. As an example for an open subshell we show, in Fig. 3, the $3d^{\uparrow}_{m=+1/2}$ state of manganese. In this case the a^+ and the a^- component contribute comparably to the total norm.

Once the radial equations (18)–(21) are solved for all relevant single-particle states, it only remains to implement this solution in the KS self-consistency cycle. The relevant points are the construction of the spherically averaged potentials and the evaluation of the total energy. Following previous algorithms,[17–19] we have chosen to perform the spherical average for the charge and magnetization densities, rather than for the potentials themselves:

$$n(r)=\frac{1}{4\pi r^2}\sum_k \Theta_k \sum_{s=\pm}[a_k^s(r)^2+b_k^s(r)^2] \qquad (50)$$

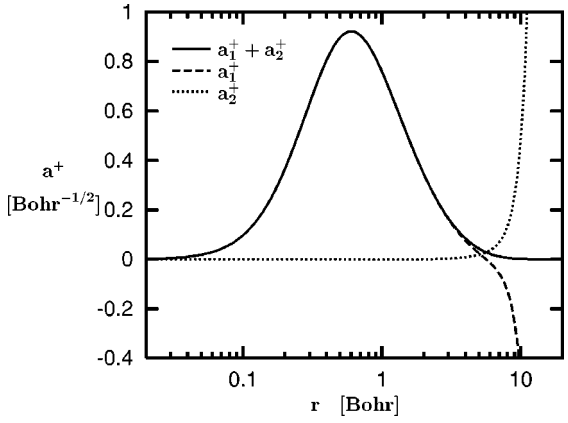

FIG. 2. Dominant component (a^+) of the $3d^{\downarrow}_{+3/2}$ state of Cu.

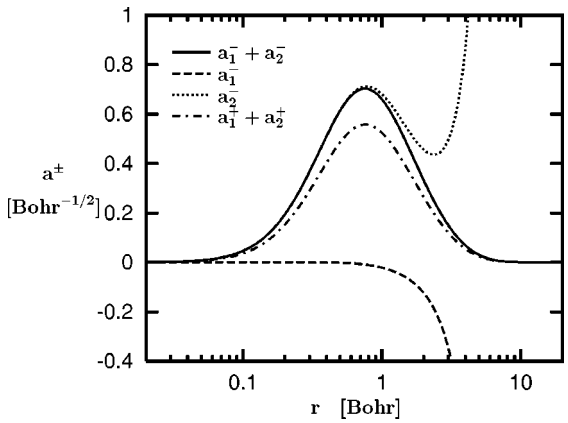

FIG. 3. $3d^{\uparrow}_{+1/2}$ orbital of Mn.

$$m_z(r)=-\frac{\mu_B}{4\pi r^2}\sum_k \Theta_k\left\{\frac{2m}{2l+1}[a_k^+(r)^2-a_k^-(r)^2]\right.$$
$$+\frac{2m}{2l+3}b_k^+(r)^2-\frac{2m}{2l-1}b_k^-(r)^2$$
$$\left.+2C_{lm}a_k^+(r)a_k^-(r)\right\} \qquad (51)$$

[$k\equiv(nlm\sigma)$ for states with $2|m|\neq 2l+1$ and $k\equiv(nlm)$ for $2|m|=2l+1$; $a_k^-=b_k^-=0$ in the latter case]. Equations (50) and (51) automatically lead to spherical potentials v_s and B_{xc}. The spherically averaged densities are also used for the evaluation of the total energy.

III. RESULTS

In this section we present a number of illustrative results and a set of reference data, obtained with the procedure described in Sec. II. The physical aspects behind the solutions of Eqs. (18)–(21) were extensively discussed in the literature, to which we refer the interested reader (see, in particular, Ref. 19).

We first compare our results with the older data in the literature, using the same xc functional in our calculations as the functional applied in the corresponding reference. Our results for the eigenvalues of the lanthanide ions Ce^{3+}–Gd^{3+} agree very well with those given by Cortona *et al.*:[17] They are essentially identical for the lighter elements, for which Ce^{3+} is given as an example (see Table I), and differ by less than 1 mH even for the heaviest ion. The corresponding ground state energies are also reasonably close, as can be seen from Table II for the case of Gd^{3+}. A similar degree of agreement is not found for the eigenvalues of the lanthanide and actinide ions of Yamagami *et al.*[19] Table I shows that the differences are of the order of 25 mH.

Ground state energies of neutral atoms have only been published by Eschrig and Servedio.[8] In these calculations the RLDA for the exchange energy of an unpolarized system[14,1] has been combined with the spin-dependence of the nonrelativistic exchange functional, $E_x[n_+,n_-]=(E_x^{RLDA}[2n_+]+E_x^{RLDA}[2n_-])/2$. In Table II we compare the corresponding results for Sn. Again, excellent agreement is found.[26]

TABLE I. $4f$ eigenvalues of Ce^{3+} [XRR (Ref. 13); vBH (Ref. 29); pw, present work].

m	σ	Θ_k	$-\epsilon_k$ (Hartree)			
			pw	Ref. 17	pw	Ref. 19
			x: XRR; c:—		x: LDA; c: vBH	
$+5/2$	$\uparrow$	1	1.0239	1.0239	1.0981	1.1231
$+3/2$	$\uparrow$	0	1.0225	1.0225	1.0968	1.1203
$+1/2$	$\uparrow$	0	1.0210	1.0210	1.0954	1.1204
$-1/2$	$\uparrow$	0	1.0194	1.0194	1.0938	1.1189
$-3/2$	$\uparrow$	0	1.0175	1.0175	1.0920	1.1170
$-5/2$	$\uparrow$	0	1.0154	1.0153	1.0898	1.1148
$-7/2$		0	1.0125	1.0125	1.0866	1.1117
$-5/2$	$\downarrow$	0	0.9954	0.9954	1.0736	1.0987
$-3/2$	$\downarrow$	0	0.9932	0.9932	1.0713	1.0965
$-1/2$	$\downarrow$	0	0.9914	0.9914	1.0695	1.0947
$+1/2$	$\downarrow$	0	0.9897	0.9898	1.0680	1.0931
$+3/2$	$\downarrow$	0	0.9883	0.9883	1.0665	1.0917
$+5/2$	$\downarrow$	0	0.9869	0.9869	1.0653	1.0904
$+7/2$		0	0.9857	0.9857	1.0641	1.0892

As an illustration of the possibilites of the new method, Fig. 4 shows the xc-magnetic field obtained for neutral gold with the LDA. The form of B_{xc} directly reflects the orbital density of the uncompensated $6s$ electron. In addition, Fig. 4 clearly exhibits the fact that the leading coefficient B_0 of expansion (24) does not vanish, as incorporated into boundary conditions (25)–(34). The absolute size of B_0 is even larger in the case of GGA's. The corresponding ground-state energy of gold is included in Table II. It differs from the energy obtained with an unpolarized calculation by 0.15 eV, a correction, which is definitively not negligible for the evaluation of dissociation or cohesive energies.

The accuracy which can be achieved with the algorithm allows a detailed investigation of the interplay between relativistic, spin, and nonlocal xc effects. As examples, in Table II we list the ground-state energies of vanadium and iron. The data for iron show that the stability of the spin-polarized ground state relative to the unpolarized state is somewhat lower in the relativistic case than in the nonrelativistic limit (122 versus 130 mH for the $3d^6\,4s^2$ configuration and the LDA). In consistency with this observation, Fig. 5 demonstrates that the relativistic treatment leads to somewhat smaller errors for the $4s \rightarrow 3d$ transfer energies than the corresponding nonrelativistic calculations, in particular for the

TABLE II. Ground-state energies of some prototype atoms: Spin-dependent vs unpolarized LDA and PW91-GGA (Ref. 15) values. NR under T_s indicates a strictly nonrelativistic calculation [VWN (Ref. 25); PZ (Ref. 30); RLDA (Refs. 14 and 1); —XRR (Ref. 13); all energies are in Hartrees].

Atom	T_s	Mode	E_x	E_c	Occupation	$-E_{tot}$
V	R	pol.	LDA	VWN	$3d^3 4s^2$	947.14566
	R	pol.	LDA	VWN	$3d^4 4s^1$	947.18279
	R	pol.	PW91	PW91	$3d^3 4s^2$	949.36423
	R	pol.	PW91	PW91	$3d^4 4s^1$	949.40562
Fe	NR	unpol.	LDA	VWN	$3d^6 4s^2$	1261.09305
	NR	pol.	LDA	VWN	$3d^6 4s^2$	1261.22329
	R	unpol.	LDA	VWN	$3d^6 4s^2$	1270.23386
	R	pol.	LDA	VWN	$3d^6 4s^2$	1270.35642
Sn	R	pol.	RLDA	PZ	$6s^2 6p^2$	6165.27109
Refs. 8 and 26	R	pol.	RLDA	PZ	$6s^2 6p^2$	6165.27113
Gd^{3+}	R	pol.	XRR	—	$4f^7$	11239.25673
Ref. 17	R	pol.	XRR	—	$4f^7$	11239.248
Au	R	unpol.	LDA	VWN	$6s^1$	19037.57102
	R	pol.	LDA	VWN	$6s^1$	19037.57646

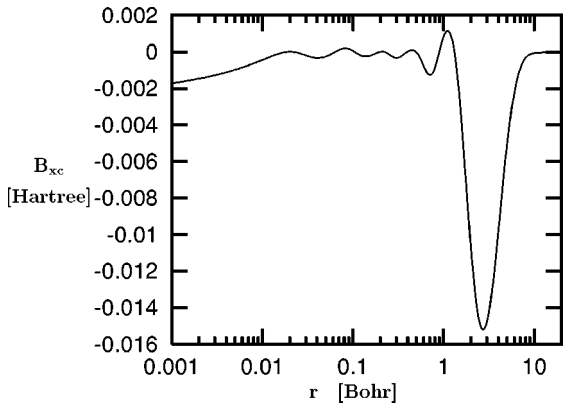

FIG. 4. Exchange-correlation magnetic potential: Au.

upper half of the $3d$ series [compare Ref. 27—as experimental reference values the $(2J+1)$-weighted interconfigurational energies of Ref. 28 have been utilized]. On the other hand, the energy gain obtained by transferring an electron from the minority spin $4s$ to the majority spin $3d$ level increases when gradient corrections are included [from 37 to 44 mH in the case of vanadium and the (Perdew-Wang 91) GGA (Ref. 15)]. As a consequence the deviations from the experimental s-d transfer energies are slightly larger for the GGA (see Fig. 5). This result indicates the limitations of these semilocal functionals.

The relevance of a magnetization-dependent treatment of spin in relativistic approximations for E_{xc} is illustrated in Table III. We list some prototype ground state energies obtained by dealing with the spin dependence of the weakly relativistic LDA for E_x (correct to order $1/c^2$) in two different ways: On the one hand, the correct magnetization-dependent form given by Xu *et al.*[13] is used via Eqs. (4) and (5). On the other hand, the form of this functional for unpolarized systems is combined with the spin dependence of the nonrelativistic exchange,

$$E_x[n_+,n_-]=\tfrac{1}{2}\{E_x^{unpol}[2n_+]+E_x^{unpol}[2n_-]\},$$

relying on Eqs. (9)–(11). Table III indicates that the differences between the energies obtained with the two approaches are rather small, in particular for heavy elements. This result

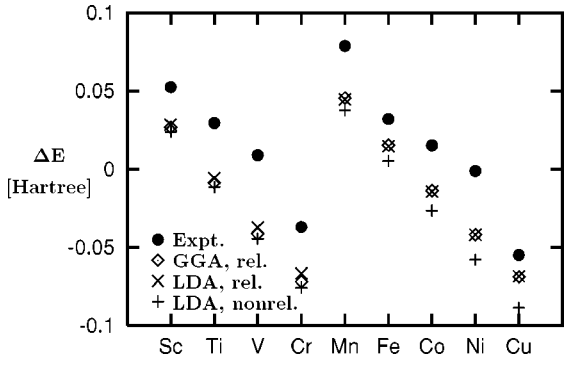

FIG. 5. $4s^2 3d^n \rightarrow 4s^1 3d^{n+1}$ transfer energies of $3d$ transition-metal elements: RSDFT results on the basis of the LDA (Ref. 25) and PW91-GGA data (Ref. 15) as well as nonrelativistic LDA data versus experiment [for the latter the $(2J+1)$-weighted interconfigurational energies of Ref. 28 have been utilized].

TABLE III. Dependence of atomic ground-state energies $(-E_{tot})$ on the treatment of spin: Comparison of the correct magnetization-dependent form of the weakly relativistic LDA [XRR (Ref. 13)] and the combination of the unpolarized, weakly relativistic LDA functional with the spin-dependence of the nonrelativistic E_x (all energies are in Hartrees).

Atom	XRR	Nonrel. spin
Cr	1045.94224	1045.94204
Fe	1267.11644	1267.11618
Eu	10814.45737	10814.45613
W	16101.78182	16101.78179
Au	21599.62664	21599.62664
U	27925.39595	27925.39590
Am	30335.91140	30335.91099

clearly supports the combination of relativistic exchange functionals for unpolarized systems [as, e.g., the relativistic GGA (Ref. 16)] with the spin dependence of the nonrelativistic exchange in applications to polarized systems.

As an additional demonstration of the general applicability of the scheme for the solution of Eqs. (18)–(21), in Fig. 6 we plot the percentage deviation of the resulting first ionization potentials (IP's) from experiment for the complete periodic table. In Fig. 6 the nonrelativistic LDA (Ref. 25) has been used (the IP's have been evaluated as ground-state energy differences, utilizing the experimental ground-state configuration). The spin-dependent approach is compared with an unpolarized treatment. It is obvious that the spin-dependent scheme yields much more accurate IP's, in particular for light atoms and lanthanides. On the other hand, only minor differences are observed for the $3d$ elements. Similar results are found in the case of the PW91-GGA (Fig. 7). This is consistent with the results for the s-d transfer energies.

In Table IV we list the ground state energies of all neutral atoms up to $Z=102$ obtained with the LDA and two frequently applied GGA's, on the basis of the experimental ground state configuration. These numbers can serve as atomic reference energies in the calculation of dissociation or cohesive energies.

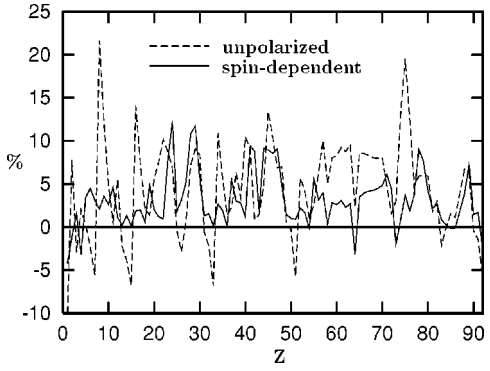

FIG. 6. Ionization potentials of neutral atoms: Percentage deviation of spin-dependent and unpolarized LDA results from experiment (Ref. 33).

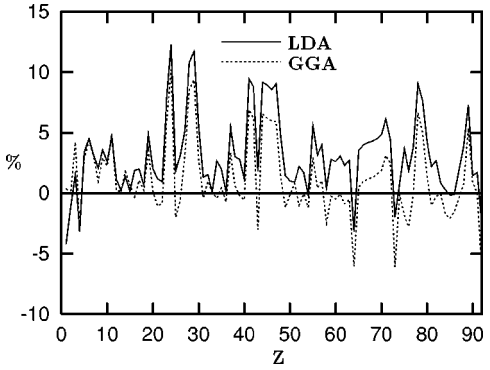

FIG. 7. Ionization potentials of neutral atoms: Percentage deviation of spin-dependent PW91-GGA results from experiment (Ref. 33) vs LDA data.

IV. SUMMARY

An algorithm for a solution of the single-particle equations of RSDFT for open-subshell atoms, introduced in Sec. II, is found to be both very robust and generally applicable. The first property results from the identification of an additional node quantum number for the distinction between spin-up and spin-down states, which allows the use of the standard numerical shooting strategy to obtain convergence for a given state. In fact, this scheme is sufficiently stable to treat all core and valence states on equal footing. The general applicability is due to the use of extended boundary conditions, which also account for nonvanishing magnetic xc fields at the nuclear site. The scheme can thus be used directly in standard band structure codes.

On the basis of this algorithm we have shown that RSDFT yields more accurate *s*-*d* transfer energies for the 3*d* elements than nonrelativistic spin-density-functional theory, without, however, really resolving the basic difficulties to reproduce these quantities with LDA or GGA functionals.[27] A case in point is vanadium, for which the RSDFT incorrectly predicts a $3d^4 4s^1$ ground state for both types of xc functionals. Nevertheless, spin-polarized relativistic GGA calculations currently represent the optimum DFT approach to magnetic systems. For this reason we have provided a complete set of atomic ground-state energies for future reference.

We have also analyzed the relevance of a magnetization-dependent treatment of the spin degree of freedom in the relativistic E_{xc}. For the only functional for which the correct magnetization-dependent form is known (the weakly relativistic LDA exchange), exact results have been compared with those of an approximate scheme, in which the form of this functional for unpolarized system is combined with the spin dependence of the nonrelativistic exchange. It has been found that the two approaches yield almost identical ground-state energies, thus supporting the use of the nonrelativistic spin dependence of E_{xc} in RSDFT calculations.

ACKNOWLEDGMENTS

We would like to thank V. D. P. Servedio and H. Eschrig for helpful correspondence. Financial support by the Deutsche Forschungsgemeinschaft (Grant No. Dr 113/20-3) is gratefully acknowledged.

APPENDIX: SOLUTION OF ASYMPTOTIC EQUATIONS INCLUDING B_{xc}

In order to find the asymptotic solutions of Eqs. (18)–(21) for nonvanishing B_{xc} one first of all separates the asymptotically dominant factors in $a^{\pm}$ and $b^{\pm}$ from the remainders:

$$a^{\pm}(r)=\tilde{a}^{\pm}(r)r^h e^{-\alpha r}, \tag{A1}$$

$$b^{\pm}(r)=\tilde{b}^{\pm}(r)r^h e^{-\alpha r}. \tag{A2}$$

Restricting the discussion to Eqs. (18) and (19), as differential equations for $\tilde{a}^+$ and $\tilde{b}^+$, one obtains

$$c(\partial_r-\alpha)\tilde{a}^+(r)=(2m_e c^2+\epsilon)\tilde{b}^+(r), \tag{A3}$$

$$c(\partial_r-\alpha)\tilde{b}^+(r)=-\epsilon\tilde{a}^+(r)+C_{lm}B_{xc}(r)\tilde{a}^-(r). \tag{A4}$$

Differentiation of Eq. (A3) and subsequent insertion of Eq. (A4) leads to

$$(\partial_r-2\alpha)\partial_r\tilde{a}^+(r)=-\frac{\alpha^2}{\epsilon}C_{lm}B_{xc}(r)\tilde{a}^-(r). \tag{A5}$$

The general solution of Eq. (A5) is obtained as a superposition of the general solution of the corresponding homogeneous equation,

$$\tilde{a}^+(r)=\overline{a_0^+}+\tilde{a}_0^+ e^{2\alpha r}, \tag{A6}$$

with $\tilde{a}_0^+=0$ for normalizable $a^+(r)$, and a special solution of the inhomogeneous equation:

$$\partial_r\tilde{a}^+(r)=-\frac{\alpha^2}{\epsilon}C_{lm}\int_{\infty}^{r}dr' e^{2\alpha(r-r')}B_{xc}(r')\tilde{a}^-(r'). \tag{A7}$$

Equation (A7) can be simplified by using the fact that the r'-dependence of the integrand is dominated by the decay of $e^{-2\alpha r'}$, as neither $B_{xc}(r')$ nor $\tilde{a}^-(r')$ change much over the length scale of $1/(2\alpha)$:

$$\partial_r\tilde{a}^+(r)\approx\frac{\alpha}{2\epsilon}C_{lm}B_{xc}(r)\tilde{a}^-(r) \tag{A8}$$

[recall that the B_{xc}-contribution to (A5) is only relevant if B_{xc} decays much more slowly than $a^{\pm}$]. The complete solution is thus given by

$$\tilde{a}^+(r)=\overline{a_0^+}+\tilde{a}^-(r)\frac{\alpha}{2\epsilon}C_{lm}\int_{\infty}^{r}dr' B_{xc}(r'), \tag{A9}$$

where again terms suppressed by $1/r$ or e^{-r} have been neglected.

TABLE IV. Ground-state energies ($-E_{tot}$) of neutral atoms: LDA (Ref. 25) vs PW91- GGA (Ref. 15) and PBE-GGA (Ref. 31) [all energies are in Hartrees (Ref. 32)].

	LDA	PW91-GGA	PBE-GGA
H	0.47868	0.50156	0.49999
He	2.83497	2.90014	2.89307
Li	7.34475	7.47500	7.46300
Be	14.45004	14.65087	14.63287
B	24.36107	24.63755	24.61302
C	37.48636	37.84328	37.81035
N	54.16817	54.61073	54.56773
O	74.58346	75.11146	75.05801
F	99.20716	99.82614	99.76010
Ne	128.37846	129.09377	129.01350
Na	161.66714	162.48730	162.39503
Mg	199.46049	200.38494	200.27996
Al	241.77643	242.81025	242.69215
Si	288.85159	289.99857	289.86682
P	340.85376	342.11738	341.97145
S	397.86736	399.24050	399.07912
Cl	460.13334	461.62158	461.44434
Ar	527.81780	529.42559	529.23208
K	600.57406	602.30432	602.09557
Ca	678.70298	680.55420	680.32969
Sc	762.33992	764.31159	764.06930
Ti	851.76816	853.86228	853.60145
V	947.14566	949.36423	949.08436
Cr	1048.69333	1051.04365	1050.74317
Mn	1156.36439	1158.83785	1158.51875
Fe	1270.35642	1272.95358	1272.61349
Co	1390.90098	1393.62421	1393.26234
Ni	1518.15298	1521.00469	1520.62057
Cu	1652.33534	1655.31827	1654.91020
Zn	1793.39780	1796.51371	1796.08415
Ga	1941.22253	1944.47824	1944.02698
Ge	2096.03717	2099.43590	2098.96262
As	2257.94100	2261.48607	2260.99085
Se	2426.97940	2430.66225	2430.14385
Br	2603.31988	2607.14578	2606.60400
Kr	2787.07159	2791.04474	2790.47968
Rb	2977.92162	2982.04501	2981.45770
Sr	3176.13524	3180.40759	3179.79760
Y	3381.76966	3386.19325	3385.55955
Zr	3595.05989	3599.63803	3598.98045
Nb	3816.16323	3820.90858	3820.22692
Mo	4045.16896	4050.07748	4049.37223
Tc	4282.09325	4287.15629	4286.42569
Ru	4527.15444	4532.37491	4531.61960
Rh	4780.47262	4785.85447	4785.07400
Pd	5042.19949	5047.74658	5046.94089
Ag	5312.36353	5318.07889	5317.24754
Cd	5591.01008	5596.89224	5596.03521
In	5878.05292	5884.10790	5883.22493
Sn	6173.71182	6179.94237	6179.03293

TABLE IV. (*Continued*).

	LDA	PW91-GGA	PBE-GGA
Sb	6478.07839	6484.48848	6483.55270
Te	6791.22030	6797.80216	6796.83904
I	7113.27454	7120.03361	7119.04288
Xe	7444.34787	7451.28831	7450.27004
Cs	7784.19997	7791.32503	7790.28008
Ba	8133.08937	8140.39877	8139.32674
La	8491.11732	8498.61478	8497.51480
Ce	8858.67009	8866.35196	8865.22203
Pr	9235.96003	9243.83192	9242.67267
Nd	9623.10563	9631.17032	9629.98155
Pm	10020.24734	10028.50776	10027.28928
Sm	10427.52656	10435.98572	10434.73736
Eu	10845.08611	10853.74713	10852.46873
Gd	11272.90664	11281.77201	11280.46305
Tb	11711.33988	11720.40251	11719.05982
Dy	12160.47426	12169.74299	12168.36791
Ho	12620.48353	12629.96208	12628.55449
Er	13091.52321	13101.21543	13099.77518
Tm	13573.75221	13583.66203	13582.18898
Yb	14067.33441	14077.46585	14075.95984
Lu	14572.27872	14582.63729	14581.09829
Hf	15088.69894	15099.28911	15097.71671
Ta	15616.73835	15627.56546	15625.95971
W	16156.54607	16167.61583	16165.97690
Re	16708.27579	16719.59438	16717.92247
Os	17272.03067	17283.59291	17281.88622
Ir	17848.04336	17859.85619	17858.11445
Pt	18436.49930	18448.57231	18446.79565
Au	19037.57646	19049.91433	19048.10318
Hg	19651.39495	19664.00068	19662.15449
Tl	20277.88468	20290.76681	20288.88542
Pb	20917.38869	20930.55076	20928.63387
Bi	21570.04178	21583.49471	21581.54167
Po	22236.06385	22249.80929	22247.82018
At	22915.66136	22929.70595	22927.68004
Rn	23609.05606	23623.40775	23621.34477
Fr	24316.18975	24330.85713	24328.75773
Ra	25037.42229	25052.41055	25050.27425
Ac	25772.94915	25788.26797	25786.09365
Th	26523.10816	26538.76726	26536.55478
Pa	27288.31317	27304.31708	27302.06588
U	28068.89946	28085.26058	28082.97067
Np	28865.16067	28881.88969	28879.56085
Pu	29677.47069	29694.58126	29692.21410
Am	30506.07047	30523.57335	30521.16694
Cm	31351.22918	31369.13313	31366.68599
Bk	32213.48367	32231.79236	32229.30296
Cf	33093.11914	33111.85208	33109.32091
Es	33990.56885	34009.74129	34007.16811
Fm	34906.25722	34925.88515	34923.26963
Md	35840.63401	35860.73433	35858.07611
No	36794.17732	36814.76807	36812.06676

[1] A.H. MacDonald and S.H. Vosko, J. Phys. C **12**, 2977 (1979).
[2] M.V. Ramana and A.K. Rajagopal, J. Phys. C **14**, 4291 (1981).
[3] A.K. Rajagopal and J. Callaway, Phys. Rev. B **7**, 1912 (1973).
[4] E. Engel and R. M. Dreizler, in *Density Functional Theory II*, edited by R. F. Nalewajski, Topics in Current Chemistry Vol. 181 (Springer, Berlin, 1996), p.1.
[5] E. Engel, R. M. Dreizler, S. Varga, and B. Fricke, in *Relativistic Effects in Heavy-Element Chemistry and Physics*, edited by B. A. Hess (Wiley, New York, 2001).
[6] L.M. Sandratskii, Adv. Phys. **47**, 91 (1998).
[7] L. Nordström and D.J. Singh, Phys. Rev. Lett. **76**, 4420 (1996).
[8] H. Eschrig and V.D.P. Servedio, J. Comput. Chem. **20**, 23 (1999).
[9] P. Strange, H. Ebert, J.B. Staunton, and B.L. Gyorffy, J. Phys.: Condens. Matter **1**, 2959 (1989); T. Huhne, C. Zecha, H. Ebert, P.H. Dederichs, and R. Zeller, Phys. Rev. B **58**, 10 236 (1998).
[10] E. Engel, A. Facco Bonetti, S. Keller, I. Andrejkovics, and R.M. Dreizler, Phys. Rev. A **58**, 964 (1998).
[11] M.V. Ramana and A.K. Rajagopal, J. Phys. C **12**, L845 (1979).
[12] A.H. MacDonald, J. Phys. C **16**, 3869 (1983).
[13] B.X. Xu, A.K. Rajagopal, and M.V. Ramana, J. Phys. C **17**, 1339 (1984).
[14] A.K. Rajagopal, J. Phys. C **11**, L943 (1978).
[15] J.P. Perdew, J.A. Chevary, S.H. Vosko, K.A. Jackson, M.R. Pederson, D.J. Singh, and C. Fiolhais, Phys. Rev. B **46**, 6671 (1992).
[16] E. Engel, S. Keller, and R.M. Dreizler, Phys. Rev. A **53**, 1367 (1996).
[17] P. Cortona, S. Doniach, and C. Sommers, Phys. Rev. A **31**, 2842 (1985); P. Cortona, Phys. Rev. B **40**, 12 105 (1989).
[18] H. Ebert, J. Phys.: Condens. Matter **1**, 9111 (1989).
[19] H. Yamagami, A. Mavromaras, and J. Kübler, J. Phys.: Condens. Matter **9**, 10 881 (1997).
[20] J. Forstreuter, L. Steinbeck, M. Richter, and H. Eschrig, Phys. Rev. B **55**, 9415 (1997).
[21] D.R. Hartree, *The Calculation of Atomic Structures* (Wiley, New York, 1957).
[22] The inclusion of higher-order contributions to the small-r expansions (25)–(29) and (30)–(34) simplifies the solution of Eqs. (18)–(21) in the case of finite nuclei. The corresponding coefficients can be determined from Eqs. (18)–(21) as functions of $v_{-1}, v_0, \ldots$ and $B_0, B_1, \ldots$ and l, as well as the free coefficients a_0^+ or b_0^-.
[23] A.D. Becke, Phys. Rev. A **38**, 3098 (1988).
[24] E. Engel, J.A. Chevary, L.D. Macdonald, and S.H. Vosko, Z. Phys. D: At., Mol. Clusters **23**, 7 (1992).
[25] S.H. Vosko, L. Wilk, and M. Nusair, Can. J. Phys. **58**, 1200 (1980).
[26] The ground-state energies originally published in Table I of Ref. 8 suffered from a minor coding error, which has now been corrected [V.D.P. Servedio (private communication)]. The corresponding value given in Table II represents the corrected energy of Sn.
[27] J.B. Lagowski and S.H. Vosko, Phys. Rev. A **39**, 4972 (1989).
[28] J. Sugar and C. Corliss, J. Phys. Chem. Ref. Data Suppl. 2 **14**, 1 (1985).
[29] U. von Barth and L. Hedin, J. Phys. C **5**, 1629 (1972).
[30] J.P. Perdew and A. Zunger, Phys. Rev. B **23**, 5048 (1981).
[31] J.P. Perdew, K. Burke, and M. Ernzerhof, Phys. Rev. Lett. **77**, 3865 (1996); **78**, 1396(E) (1997).
[32] The speed of light had been set to $c = 137.0359895$ a.u.
[33] D.R. Lide, *Handbook of Chemistry and Physics 1996-97* (CRC Press, Boca Raton, FL, 1996).